

Discovering Hidden Faults Under The Oil Field Of Alborz Anticline In Qom, Iran

Hamid Reza Moradi¹, Vahid Hosseinitoudeshki²

^{1,2}Department of Geology, Science and Research Branch, Islamic Azad University, Tehran, Iran

Abstract—In this study we tried to find hidden faults on Alborz Anticline located in Qom basin in Iran. To identify the hidden faults, first, the airborne geophysical map was georeferenced. Then the map was converted into a shape-file format using Geographic Information Systems mapping software. Next all the faults or the same magnetic lineaments were identified. These three steps were performed for the geological maps of six area in Qom basin. Finally, the shapefiles of geological mosaic map were integrated with that of airborne geophysical mosaic map, and therefore, all the faults, which were not complied with magnetic lineaments were introduced as hidden faults. Our investigation showed that there are 10 hidden faults including eight possible faults and two blind thrust faults in oilfield of Alborz Anticline. The average shear strain in Qom area was about 1.6 and the angle of orientation was about 13°. The basic and dominant structural trends were northwest to southeast, and the dominant trend was N130°-N135° which indicates it as a shear-compression area.

Keywords—Hidden faults; The Blind thrust fault; Alborz fault; Qom basin; Map integration

I. Introduction

Blind fault is a type of thrust faults that is hidden underneath rock layers and have not reached surface so far. Such faults, being invisible at the surface, have not been mapped by standard surface geological mapping. Sometimes they are discovered as a by-product of oil exploration seismology; in other cases their existence is not suspected. They form when a section of the Earth's crust is under high compressive stresses, due to plate margin collision, or the general geometry of how the plates are sliding past each other.

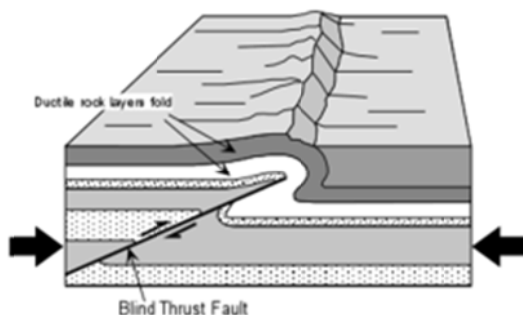


Fig. 1. Diagram of blind thrust fault (source: <http://earthquake.usgs.gov>)

There are several studies conducted in discovering hidden faults around the world using different methods. For example, Liberty et al. [1] discovered a hidden fault in Portland, Oregon using multiple high resolution geophysical techniques, including seismic reflection, ground penetrating radar (GPR), and magnetic methods, with regional geological and geophysical surveys. According to them, there are three potentially active faults in the vicinity of downtown Portland. Bonforte et al. [2] used soil gases and SAR measurements to find hidden faults on Mt. Etna, Italy. Coupling SAR with soil gas prospecting methods proved to be a powerful tool in detecting hidden active faults. Rudersdorf et al. [3] detected the hidden fault in the Gobi Desert (Inner Mongolia, China) using microtremor analysis, GPR and SQUID-supported transient electromagnetics. Micrometer analysis showed a significant offset of the basement topography, and GPR indicated shallow faulting. Johnová et al. [4] searched for hidden faults on the SE flank of the Mt. Etna volcano using radon gas and measurements of soil gas radon concentrations. They mentioned that although there are many methods for investigating tectonic structures, many faults remain hidden. They believed that the blind faults can endanger the life and property of people. The slopes of volcanoes are covered with such hidden faults, near which strong earthquakes and gas releases can appear. Drozd and Drozd [5] investigated the hidden faults in Ukraine to develop computer systems for providing safety-related instrumentation and control systems. According to them, the hidden faults do not allow ensuring functional safety by construction of fault tolerant digital component without consideration of their check ability.

In this study our purpose is to identify the hidden faults under oilfield of Alborz anticline in Qom located in the north of Qom in Iran. First we find surface faults and then by integrating with magnetic lineaments on the geologic maps, we reveal the hidden faults. Finally we comply them with the deformation model of the study area.

II. Study Area

I. Qom section

Qom area is located in the central part of Iran plate wherein Eocene and younger sediments such as volcanic and volcanic/clastic rocks with carbonate and marine evaporates have been deposited [6, 7]. Qom Formation mainly contains shelf - upper slope carbonate platform with a Rupelian to Burdigalian age. After oil was discovered in porous bioclastic

limestones in 1934 [8-10] the Qom formation attracted the researchers but geological research of the Qom Formation mostly remained limited to the Qom Basin [11]. In Qom-Saveh basin, Qom sediments include Marl, carbonate, sandy carbonate, bituminous shales with anhydrite layers. There is six lithostratigraphic units including basal limestone, sandy marls, alternating marls and limestones, evaporites, green marls, and top limestone [12]

II. Alborz fault

Alborz fault is located in the north of Qom. Given the importance of Alborz fault in terms of the formation of the structure of Qom area, the fault is formerly called Alborz thrust by the Geologists working at National Iranian Oil Company (NIOC). The fault has a geometry of N 135/75 SW. following the excavation carried out by NIOC, it was determined that the fault has found a shallower slope, and that the fault is horizontal in high evaporation deposits of Qom formation [13]. Harvesting fault indicators in the Alborz fault zone (En echelon fault, striations, and waterways movement) shows that the reverse fault movement component is left to right. The fault shear zone is about 200 meters, and its longitudinal zone is about 30 km. these zones push the Miocene units on the Pliocene - Quaternary sediments. Using key layers displaced in drilling wells, the slope movement of the fault is equal to 1600 m, the rise is 4, and the northward horizontal movement of the fault is calculated to be 1250 m [14].

Alborz fault has two different movements. The former movement is right-oblique slip, and the latter movement is left- oblique slip. According to Nogol Sadat [15], all the structures existing in Central Iran are related to the right-lateral shear movement of Arabian plate compared to that of Eurasia, and all the structures are affected by the right- lateral shear motion of Arabian plate compared to that of Eurasia. Alborz fault, due to right-lateral shear movement of Arabic plated compared to that of Iranian plate since the Miocene, is created as a reverse fault with a right-lateral shear component. Geometry of the curves of Alborz anticlinal axis and right-lateral faults, created by the movement of transverse joints, are evidences of this mechanism. The structures are created because they are placed in the shear zone between the Alborz and Qom faults. The faults, found in this zone, are likely to reach the Alborz fault at depth or are likely to have shallower depth.

Alborz Anticline is beyond the Alborz fault wall, and its axis has a double-direction plunge towards southeast and northwest. The slope of the southern flank varies between 7 to 45 degrees such that the slope is reduced gradually from the southwest to the northeast along the shear structure. Qomroud River passes through the Alborz anticline. Alborz fault activity has caused a rift in this area such that the River has rifted the bedrock deeply. Severe erosion of the River has led to large, elliptical, alluvial fan in the northern plains of Alborz fault. The alluvial fan, itself, is rifted by the reactivation of the Rive, and it has been displaced left-laterally. Furthermore, Alborz fault thrust has caused

the Quaternary units to be inclined in hanging wall and footwall.

III. Research Method

This study aims to discover the blind faults under oilfield of Alborz anticline in Qom, Iran which was conducted in 2014. First we find surface faults and then by integrating them with magnetic lineaments, we find the hidden faults.

A. Identifying the existing faults on the airborne geophysical mapping of Qom section

The 1:50000-scale airborne geophysical mapping of Qom section was prepared from Institute of geophysics of Tehran University in Iran. By using GIS, this map was geo-referenced to be in its actual spatial location.



Fig. 2. Airborne geophysical map of Qom

This map then was converted into a shapefile format and all of its existing faults (magnetic lineaments) which are shown with blue lines in figure 3, were extracted.

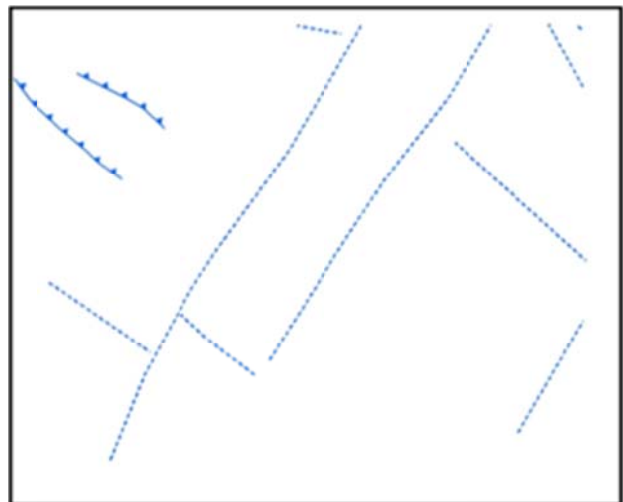


Fig.3. Shapefile of airborne geophysical map of Qom

B. Identifying surface faults on Qom basin

Six geological maps of Qom, Farmahin, Salafchegan, Kahak, Tafresh, and Arak areas in Qom basin that comply with the airborne geophysics map were prepared from the Geological Survey of Iran (GSI) with a scale of 1:100000; and then they are georeferenced using GIS. Also, the 1:100000-scale geological map of Aran region was prepared from the GSI. This region which is located near Kahak, is outside of the study area, but due to the importance of the faults existing in Kahak and its extension to the Aran, the map of Aran region was also georeferenced. In next step, all the six georeferenced maps were converted into a shapefile format, and all the surface faults existing in each map (including normal, reverse, thrust, strike-slip and possible faults) are plotted on the shapfile. Figures 4 and 5 show the mosaic of the geologic map of Qom basin and the shapefile of this mosaic map respectively. All the surface faults are denoted by red lines.



Fig. 4. Geologic mosaic map of Qom basin

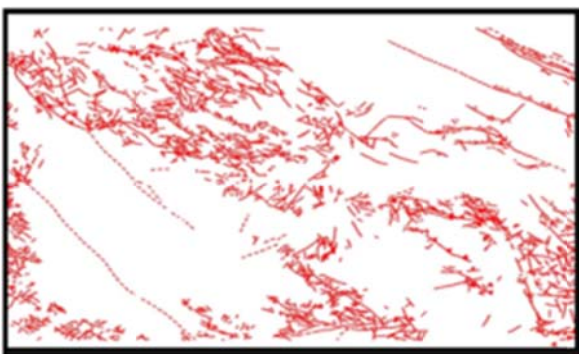


Fig. 5. Shapefile of geologic mosaic map of Qom basin

IV. Results

A. Identifying the hidden faults in Qom basin

The geological mosaic map of Qom basin (Fig. 4) is integrated with the airborne geophysical map of Qom (Fig. 2) and is presented as figure 6. Then the shapefile of airborne geophysical map (Fig. 3) is combined with Shapefile of geologic mosaic map (Fig.5) and is resulted as Figure 7.



Fig.6. Integrated geological mosaic map of Qom Basin and the airborne geophysical map of Qom

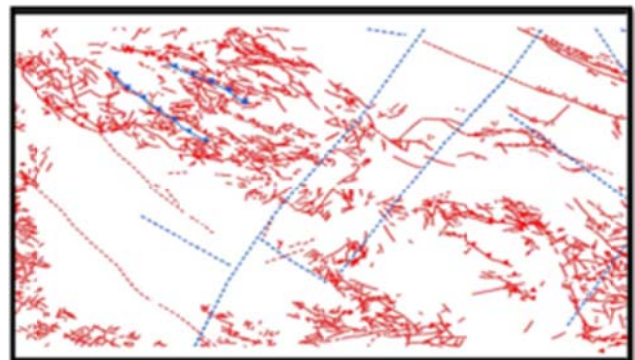


Fig. 7. Integrated shapefile of geological mosaic map of Qom basin and shapefile of the airborne geophysical map of Qom

By integrating surface faults of Qom basin with magnetic lineaments of Qom section the faults that are seen on the airborne geophysical map but have no compliance with the faults shown on geological mosaic map were identified as the blind or hidden faults. These hidden faults are shown with green lines in figure 8.

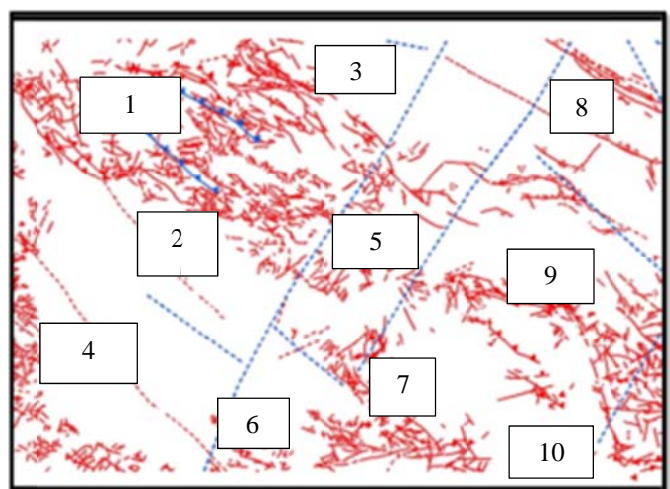


Fig. 8. Discovered hidden faults in Qom Basin

A. Investigating the orientation of hidden faults existing in Qom area Transpressional strain model

After detecting the hidden faults in Qom Basin, we investigated the structural trend of the faults, and were complied with Tabriz-Bazman zone structural trends. As can be seen in Figure 8, the blind faults have basic and dominant northwest-southeast structural trends. In addition, the dominant trend of the region ranges from N130° to N135° which is known as a compression-shear zone. To match these structural trends to those existing in the region; first, the structural trends of Qom section should be considered. In average, the general trend of Qom section is NW -SE. Subsequent formation of structure of basin deposits is the result of right-lateral shear motion mechanism with compression. Since the effect of axial surface of Qom anticline is curved and Z-shaped with a right-lateral slip, it indicates the effect of right-lateral component. So, the walls of the sediment basin are considered as oblique to the main stress so that the main stress, when is facing with the walls, be divided into two normal (vertical) and shear (parallel to wall). In this case, we have a convergent strike-slip zone or a Transpressive zone.

Current models suggest that structural orientations within the zones depend on not only the magnitude of shear strain but also the degree of convergence or divergence. The transpressional strain mode of Sanderson and Marchini [16] is used in this study which relates the three-dimensional strain of a domain undergoing distributed horizontal shear between two parallel vertical boundaries to the magnitude of shear and convergence (or divergence) of the boundaries. Figure 9 depicts the transpressional strain model where α^{-1} is the convergence across the zone, parallel to the y-axis, α is the vertical thickening, parallel to the z-axis, and y is the horizontal shear strain, parallel to the x-axis.

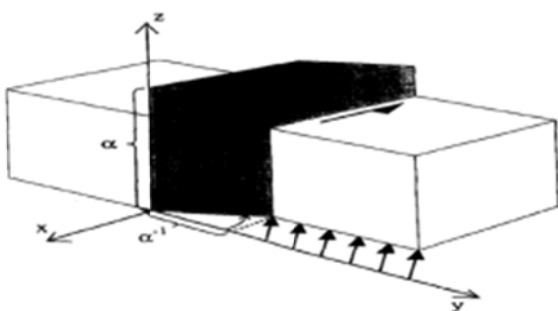


Fig. 9. Transpressional strain model adapted from [17]

In convergent strike-slip, a horizontal ellipse is formed. The size and orientation of the ellipse are shown by S_{Hmax} , S_{Hmin} and ϕ . S_{Hmax} is one-half of the length of the major axis of the horizontal ellipse, and S_{Hmin} is one-half of the length of the minor axis of the ellipse and ϕ is the orientation of the long axis measured from the x-axis [17]. In convergence strike slip zones, both the value and orientation of the strain can be calculated; as a result, the orientation and geometry of the structural components can be determined. For this

purpose, first, the convergence factor of the study area should be determined.

1). Convergence factor

The Convergence factor (R) is defined as the ratio of convergence component across the shear zone to the strike-slip component. The positive R indicates convergence component and the negative R shows the divergence component.

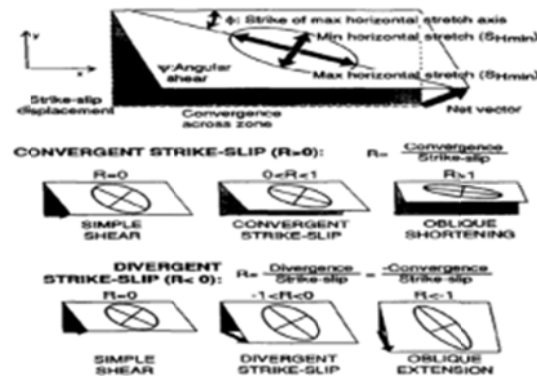


Fig. 10. The horizontal strain parameters adapted from [17]

By decomposing the main stress (σ_1) to compressive (σ_n) and shear (τ) components, it was found that the compressive component is greater than shear component. Using the trigonometric relations of $\sigma_n = \sigma_1 \cos 2\theta$, the relative values of both compression and shear components can be obtained as follows:

$$\sigma_n = \sigma_1 \frac{1 + \cos 2\theta}{2} \rightarrow \sigma_n = \sigma_1 \frac{1 + \cos(2 \times 20^\circ)}{2} = 0.883\sigma_1$$

$$\tau = \sigma_1 \sin \theta \cos \theta \rightarrow \tau = \sigma_1 \sin 20^\circ \cos 20^\circ = 0.321\sigma_1$$

$$\frac{\sigma_n}{\tau} = \frac{0.883\sigma_1}{0.321\sigma_1} = 2.75$$

Therefore, it became clear that the ratio of compressive component (convergence) to shear component (strike-slip) in the study area is equal to 2.75 which is the convergence factor. Now, if we can determine the orientation of horizontal strain ellipse in the area, we will be able to determine the primary orientation of all the existing structures. For this purpose, we can read figures 11 and 12. In these figures, R, orientation of horizontal strain ellipse, and other parameter of strain ellipse (S_{Hmax} and S_{Hmin}) are related to each other. Therefore, by calculating the R (2.75 for Qom area) if we can determine S_{Hmax} and S_{Hmin} , we will be able to determine orientation of strain ellipse (ϕ).

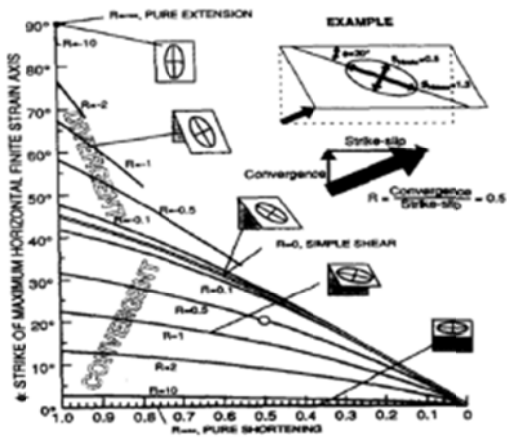


Fig. 11. Nomogram for parameters of R , ϕ and S_{Hmin} . The strain increases from left to right. The white dot shows the correct location for the example [17]

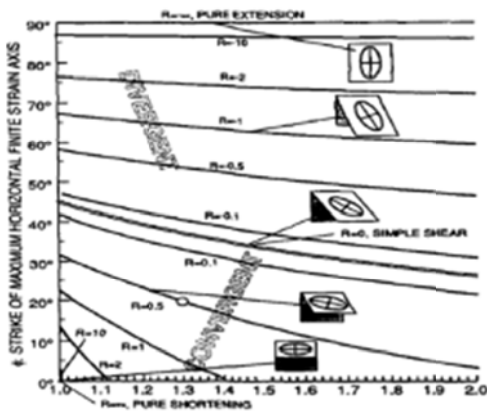


Fig. 12. Nomogram for parameters of R , ϕ and S_{Hmax} . The strain increases from left to right. The white dot shows the correct location for the example shown in FIG. 10[17]

Our investigation showed that the average shear strain in Qom area is about 1.6, S_{Hmax} is about 1, and its S_{Hmin} is about 0.6. By using R , S_{Hmax} and S_{Hmin} values in figures 11 and 12, we can obtain the ϕ for Qom section which is about 13° . It means that due to the effect of the common function of both compressive and shear stresses on the area and the creation of a convergent strike-slip zone, Qom Anticline and the reverse faults existing in the area have been created with an angle of 15° to the domain wall (trend = N 115°), and due to continuation of the deformation phase, Qom Anticline and the reverse faults existing in the area have had a right-lateral slip and have become curved with a Z-shape. The normal faults formed perpendicular to the axis of the folds, and the Riedel shears with the angles is shown in figure 13.

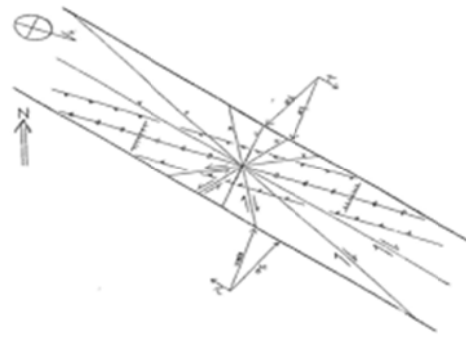


Fig. 13. Convergent strike-slip deformation model for the study area; the horizontal strain ellipse with an angle of about 15° to the wall and different structures

According to the structural trend that we found, and the integration of hidden faults with the deformation model obtained for the study area, the following trends are determined for the hidden faults of Qom area (see Fig. 14):

- Blind thrust faults No.1 and 2: are exactly complied with the thrust trends of the deformation model.
- Possible hidden faults No. 4, 6 and 9: complied with thrust trends of the deformation model. Most likely, these faults are thrust faults.
- Possible hidden fault No.7 complied with T-trend of the deformation model, and the hidden fault No. 8 which is complied with P-trend of the model.
- Possible hidden fault No. 10 complied with the normal trends of the deformation model. Most likely, this possible hidden fault is a normal fault.

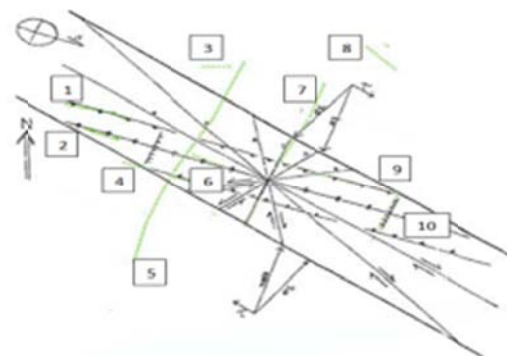


Fig. 14. The integration of hidden faults of Qom basin with its deformation model

V. Conclusion

In this study we attempted to discover the hidden faults in Qom basin, in Iran using map integration technique. Our results showed that Qom basin has 10 hidden faults (8 possible faults and two blind thrust faults). According to the analysis carried out in Qom area, we found that the average shear strain in Qom area was about 1.6. Also, the orientation value was about 13° . The basic and dominant structural trends were NW-SW, although some other trends were found; The dominant trend was N 130° - N 135° .

Integration of our found hidden faults with the deformation model of the area showed that three possible hidden faults were complied with the thrust trends of the deformation model and it appears to be thrust faults. Also, two possible blind faults were in complied with T and P-trends of the deformation model. Finally we found out that there was one possible hidden fault complied with the normal trends of the model which is mostly a normal fault.

Reference

[1]. Liberty, L. M., Hemphill-Haley, M. A, and Madin, I. P. The Portland Hills Fault: uncovering a hidden fault in Portland, Oregon using high-resolution geophysical methods. *Tectonophysics*, 2003; 368(1):89-103.

[2]. Bonforte, A., Federico, C., Giammanco, S., Guglielmino, F., Liuzzo, M., & Neri, M. Soil gases and SAR measurements reveal hidden faults on the sliding flank of Mt. Etna (Italy). *Journal of volcanology and geothermal research*, 2013, pp.251, 27-40.

[3]. Rudersdorf, A., Hölz, S., Torgoev, A., Havenith, H. B., and Reicherter, K. R. Hidden faults in the Gobi Desert (Inner Mongolia, China) revealed by microtremor analysis, ground-penetrating radar and SQUID-supported transient electromagnetics. *Conference Paper, EGU General Assembly Conference Abstracts*, 2013; 15: 9543

[4]. Johnová, K., Thinová, L., and Giammanco, S. Revealing the hidden faults in the SE flank of Mt. Etna using radon in-soil gas measurement. *Journey of Radiation protection Dosimetry*, 2014; 160(1-3): 70-73

[5]. Drozd, M., and Drozd, A. Safety-related instrumentation and control systems and a problem of the hidden faults. In *Digital Technologies (DT)*, IEEE: 10th International Conference on, 2014, pp.64-67

[6]. Bina, M. M. Bucur, I., Prevot, M., Meyerfeld, Y., Daly, L., and Cantagrel, J. M. Palaeomagnetism, petrology and geochronology of Tertiary magmatic and sedimentary units from Iran. *Journal of Tectonophysics*, 1986; 121:303–329

[7]. Berberian, M., and King, G. C. P. Towards the Paleogeography and tectonic evolution of Iran. *Canadian Journal of Earth Sciences*, 1981; 18(2):210-265.

[8]. Mostofi R, Gansser A. The story behind the 5 Alborz. *Oil Gas J* 1957; 55:78–84

[9]. Abaie IL, Ansari HJ, Badakhshan A, Jaafaki A. History and development of the Alborz and Seraih fields, central Iran. In: *Proc 6th world petrol conf*, Frankfurt, 1963, pp 1–111.

[10]. Rosenberg R. Qum-1956: a misadventure in Iranian Oil. *Bus Hist Rev* 1975; 49:81–104

[11]. Reuter, M., Piller, W. E., Harzhauser, M., Mandic, O., Berning, B., Rogl, F., Kroh, A., Aubry, M.-P., Wielandt-Schuster, U. and Hamedani, A. The Oligo-Miocene Qom Formation (Iran): Evidence for an early Burdigalian restriction of the Tethyan Seaway and closure of its Iranian gateways. *International Journal of Earth Sciences*, 2009; 98(3): 627-650

[12]. Furrer MA, Soder PA. The Oligo-Miocene formation in the Qum region (Iran). In: *Proc 4th World Petroleum Congress*, Roma, Italia, 1955.

[13]. Baghbani, D., Elahyari, M., and Shakeri, A. Investigating Qom sedimentary basin and evaluating its hydrocarbon potential (Central Iran). *National Iranian Oil Company, Geology Report*, 1996; No. 18: 38

[14]. Omid, P. Structural Curve Analysis of Alborz Anticline (North Qom). *Master Thesis*, TarbiatModarres University, Tehran, 1980..

[15]. Nogol Sadat, M.A.A. Shear Areas and Structural Curve in Iran. *the Structural Analytic Achievements of Qom Area*, Report No. 55, Tehran: Geological Survey of Iran, 1985.

[16]. Sanderson, D. J. & Marchini, W. R. D. Transpression. *J. Struct. Geol* 1984; 6,449-458.

[17]. Krantz, R. W. The transpressional strain model applied to strike-slip, oblique-convergent and obliquely divergent deformation. *Journal of Structural Geology*, 1995; 17: 1125- 137.